

Finding Efficient Trade-offs in Multi-Fidelity Response Surface Modeling

Sander van Rijn  · Sebastian Schmitt  · Matthijs van Leeuwen 
 · Thomas Bäck 

the date of receipt and acceptance should be inserted later

Abstract In the context of optimization approaches to engineering applications, time-consuming simulations are often utilized which can be configured to deliver solutions for various levels of accuracy, commonly referred to as different fidelity levels. It is common practice to train hierarchical surrogate models on the objective functions in order to speed-up the optimization process. These operate under the assumption that there is a correlation between the high- and low-fidelity versions of the problem that can be exploited to cheaply gain information. In the practical scenario where the computational budget has to be allocated between multiple fidelities, limited guidelines are available to help make that division. In this paper we evaluate a range of different choices for a two-fidelity setup that provide helpful intuitions about the trade-off between evaluating in high- or low-fidelity. We present a heuristic method based on sub-sampling from an initial Design of Experiments (DoE) to find a suitable division of the computational budget between the fidelity levels. This enables the setup of multi-fidelity optimizations which utilize the available computational budget efficiently, independent of the multi-fidelity model used.

Keywords multi-fidelity simulation problems · design of experiments · error grids · hierarchical surrogate models · co-kriging

S. van Rijn , M. van Leeuwen , T. Bäck 
 Leiden University, The Netherlands
 E-mail: s.j.van.rijn@liacs.leidenuniv.nl

S. Schmitt 
 Honda Research Institute Europe, Offenbach am Main, Germany

1 Introduction

When dealing with simulation based optimization problems in engineering applications, the runtime cost of each evaluation is typically the most restrictive aspect of a successful approach. Surrogate models are often used to reduce the total computational load by learning trends from previous evaluations. But the computational cost for single evaluations have grown too high in many modern problems for such approaches to obtain enough information necessary to train an accurate model in reasonable time.

Many such problems offer tunable accuracy and can therefore be classified as either arbitrarily tunable *variable-fidelity*, or discretely tunable *multi-fidelity* problems. In the following we focus on multi-fidelity problems specifically. Supplementing accurate high-fidelity information with cheaper low-fidelity information is regularly done by incorporating *hierarchical* (co-)surrogate models based on work by Kennedy and O'Hagan [12], such as co-kriging [7] and co-RBF [4]. These have been successfully applied in e.g. the design of ships [18] airfoils [15], satellites [25], additive manufacturing [28], and fire start determination [14].

However, it remains unclear under which conditions the inclusion of low-fidelity information in hierarchical surrogate models is actually beneficial. While previous research has shown that the correlation between high- and low-fidelity response surfaces should be fairly high (i.e., sample Pearson correlation coefficient $r > 0.9$ [26, 6]), a high correlation by itself is no guarantee for achieving added benefit of multi-fidelity models. That is, regardless of correlation, individual response surface landscapes still have a substantial impact on the final accuracy of the trained models.

Furthermore, even if a model is beneficial, how to best distribute the available computational budget between the fidelity levels is still an open question. Prior work has included experiments where models based on multiple sample sizes were compared, but most present only a limited selection of combinations, as can be seen in, e.g., the overviews by Fernández-Godino *et al.* [6,5]. Common heuristics for deciding on this division rely either on the cost ratio between fidelities or otherwise use expected information gains [8, 16, 10, 24, 1]. Of these, the former do not use any function information, while the latter are designed to be used in iterative optimization, not to gain general understanding.

In this work we empirically explore how to distribute additional computational budget over two fidelities. We focus on one-shot Design of Experiments (DoEs), by enumerating all possible combinations of a wide range of low and high fidelity samples, and fit a hierarchical model and measure its accuracy for each setup. Our approach is similar to a study by Durantin *et al.* [4] but with a much finer granularity, more sample combinations, and many more benchmark functions. By analyzing model accuracy as a function of the DoE sizes and for various benchmark functions, we aim to provide general insight into the behavior of this trade-off.

We recognize that using an enumeration procedure to obtain this information is far too computationally expensive in terms of problem evaluations for practical settings. Therefore, we present a method using subsampling that draws smaller DoEs from an initial DoE to avoid performing any new evaluations. Using these subsampled DoEs we approximate the accuracy trend results and show a high correlation between these results and those from the original full enumeration.

We present a heuristic which utilizes the information gained from the subsampling approach to predict a beneficial split of the number of high and low-fidelity samples for a given computational budget. This allows for an efficient use of the available computational resources for the multi-fidelity modeling approach to optimization.

All files for this work are archived on Zenodo [20,23]. The  and  icons under each figure link to the source code on GitHub [19] and full versions on FigShare [22]. The rest of this paper is structured as follows: Section 2 provides background definitions, Section 3 contains the problem statement, Section 4 describes the proposed methods, Section 5 presents the experiments, results and reproducibility details, and concludes with Section 6.

2 Background

In this section we define the terms and methods that are used in the remainder of this article.

2.1 Surrogate Modeling

In many situations it is useful to create a continuous model (often called response surface or surrogate model) of the input–output relation of some process, which we will refer to as a ‘*function*’ from now on. By fitting a regression model to a dataset of input–output pairs of that function, a good approximation can be created of the target function if the right type of model is chosen and enough data is available. In e.g., optimization settings, such a model can then be used as a surrogate for the actual function to give a rough estimate of the true output for an untested input. This is especially useful if it takes a long time to calculate such a true output.

2.2 Design of Experiments

A standard approach for systematically sampling a set of input parameter configurations in order to create a dataset of input–output pairs of given function is referred to as Design of Experiments (DoE) [3]. The goal when choosing such a dataset is to cover the input-space of the function in such a way that the created model is as good as it can be, whether on a local or global scale. How large the search space is and how much computational effort can be expended on this depends on each individual problem setting. However, a full factorial design (i.e., grid search) is usually out of the question due to relatively high dimensionality and high computational cost. In this work, we use the common Latin Hypercube Sample (LHS) strategy. This technique tries to create a sample such that the samples are evenly distributed over the search space, while avoiding the reuse of coordinate values for a dimension.

2.3 Multi-Fidelity Problems

A multi-fidelity problem is an optimization/simulation problem that is available in multiple *fidelities*, i.e., accuracy levels. In real-world Computational Fluid Dynamics (CFD) simulations of, e.g., airfoils, these fidelities could correspond to different mesh sizes or simulation types. A *low*-fidelity simulation would use a coarse mesh or potential flow solver, and thus give lower accuracy, but be faster to calculate, while a *high*-fidelity simulation would use a finer mesh or Reynolds-averaged Navier-Stokes (RANS) simulation and therefore be more accurate while taking longer to calculate.

In the following, we will use $f_h : \mathcal{X} \rightarrow \mathcal{Y}$ and $f_l : \mathcal{X} \rightarrow \mathcal{Y}$ to denote the high- and low-fidelity levels of a simulator, abstractly represented by the function f that maps input vectors $\mathbf{x} \in \mathcal{X}$ onto outputs $\mathbf{y} \in \mathcal{Y}$.

2.4 Additive Hierarchical Surrogate Models

To make use of the multiple sources of information in a multi-fidelity problem, an additive model-structure has been proposed by Kennedy and O'Hagan [12]:

$$z_h(\mathbf{x}) = \rho z_l(\mathbf{x}) + \delta(\mathbf{x}) \quad (2.1)$$

Here, $z_h(\mathbf{x})$, and $z_l(\mathbf{x})$ are the high- and low-fidelity surrogate models at point \mathbf{x} respectively, for approximating $f_h(\mathbf{x})$ and $f_l(\mathbf{x})$. ρ is a regression parameter, and $\delta(\mathbf{x})$ is the difference model at point \mathbf{x} , which improves the low-fidelity prediction by additive correction.

Without loss of generality, we consider simplified additive models where the regression parameter $\rho = 1$. We create independent models for z_l and δ , where z_l models the lowest accuracy information source f_l , and a separate model δ predicts the differences between the high- and low-fidelity responses $f_h(\mathbf{x}) - f_l(\mathbf{x})$.

2.5 Multi-Fidelity Design of Experiments

In a multi-fidelity setting, where we train a difference model between high and low fidelity functions, we would like to have overlapping DoEs for low and high fidelity models where all high fidelity samples are also included in the low fidelity DoE. Additionally, each DoE should still cover the search space efficiently and therefore should be an approximate LHS itself.

In order to achieve this, we use the procedure from le Gratiet [13] to generate DoEs for the hierarchical models, which is outlined in Algorithm 1. In lines 1-2, two separate LHSs are generated. Then, for each high-fidelity point, the closest low-fidelity point is replaced by that high-fidelity point (while-loop in lines 4-9). Given the desired sizes, this method returns both a high-fidelity LHS H , and a more spread-out low-fidelity sample L which is still roughly an LHS itself. As the final outcome we arrive at a DoE which is the unity of the sets L and $H \subset L$ of low and high fidelity samples, respectively, which we denote as $\text{DoE}(H, L)$ and where the exact differences $f_h(\mathbf{x}) - f_l(\mathbf{x})$ can be computed for all $\mathbf{x} \in H$ and used as training set for the difference model δ . Figure 2.1 illustrates this procedure for a 2-dimensional DoE with $n_h = |H| = 10$ and $n_l = |L| = 20$.

3 Problem Statement

The fundamental question we address in this work is: how should a given additional computational budget be distributed among multiple fidelities? Especially, in the context of computationally expensive simulation problems where the overall evaluation budget is constrained,

Algorithm 1 Multi-Fidelity LHS [13]

Require: $n_l \geq n_h + 1$

- 1: $H \leftarrow \text{LHS}(n_h)$ ▷ Independent samples per fidelity
- 2: $L \leftarrow \text{LHS}(n_l)$
- 3: $L', H' \leftarrow \emptyset$
- 4: **while** H not empty **do**
- 5: $\mathbf{h}, \mathbf{l} \leftarrow \arg \min_{\mathbf{h} \in H, \mathbf{l} \in L} \|\mathbf{h} - \mathbf{l}\|$ ▷ Find closest pair
- 6: $H' \leftarrow H' \cup \mathbf{h}$
- 7: $L' \leftarrow L' \cup \mathbf{l}$ ▷ Effectively adjust \mathbf{l} to \mathbf{h}
- 8: Remove \mathbf{h}, \mathbf{l} from H, L
- 9: **end while**
- 10: $L' \leftarrow L' \cup L$ ▷ Add remaining low-fid points
- 11: **return** H', L'

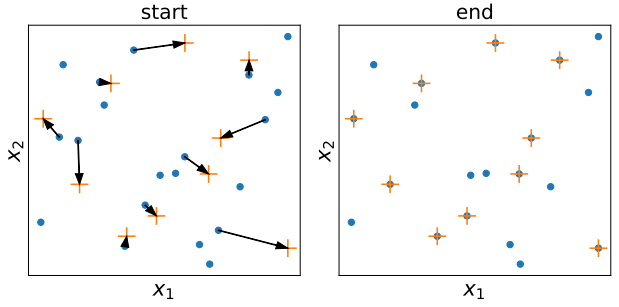


Fig. 2.1: **Illustration of Algorithm 1.** Two LHSs are created: 20 points for low-fidelity (blue circles) and 10 for high-fidelity (orange pluses). In each step the smallest distance between a high- and low-fidelity point is searched, and the low-fidelity point is moved to the closest high-fidelity point (black arrow). This is repeated until every high-fidelity point is matched

this is a highly relevant question. As a starting point we choose to address the question of how to split the high and low fidelity samples for the DoE(H, L).

The answer to this question depends on which fidelity provides the most information for its computational cost. An additional high-fidelity sample in a so-far unexplored area will definitely improve the model's accuracy. But if some number of low-fidelity samples can improve the model more with equal or lower computational cost, that might be a better choice. How much information is gained by adding another sample for a specific fidelity depends heavily on the number of samples of that fidelity already present, and on the chosen model's capacity to capture the problem's response surface.

An important quantity in determining the split between the number of high- and low-fidelity evaluations is given by the *cost ratio* $\phi = c_l/c_h \in (0, 1)$, where c_h and c_l are typical computation times associated with high- and low-fidelity evaluations, respectively. The problem can thus be stated as follows: given a fixed evaluation budget b (which is measured in high-fidelity evaluation times) and cost ratio ϕ , what are the optimal numbers

of high- and low-fidelity evaluations, i.e. the optimal division ratio $\frac{n_h}{n_l}$ that minimizes the model error and which respects the constraint that the budget is not exceeded, i.e. $n_h + \phi n_l \leq b$. As the model error, we take the Mean Squared Error (MSE) of response surface model z compared to the true function value of the highest fidelity level f_h , evaluated on a given test set $x \in T$:

$$MSE(z, T) = \sum_{x \in T} \frac{(z(x) - f_h(x))^2}{|T|}. \quad (3.1)$$

The model error is expected to have a nontrivial and in general non-linear behavior as a function of the division ratio. For the case consisting only of high fidelity evaluations, the low number of overall samples probably leads to a rather large error. On the other extreme, using only low-fidelity evaluations will also not produce an accurate model as no actual information about the true function is used. In the intermediate region, with some low-fidelity samples at the expense of a few high-fidelity evaluations it is expected to obtain a reduced model error. The details of this trade-off strongly depend on various aspects of the problem, like the structure of the high-fidelity function and the similarity between the low- and the high-fidelity functions. However, in order to learn the dominant behavior of the error as function of the number of high- and low-fidelity samples we will later employ a simple fit to the error. This will enable us to extract the global trend and allows us to formulate a heuristic which guides the distribution of additional computational budget.

4 Method

4.1 Enumeration of Multi-Fidelity DoE Sizes

To fully examine the trade-off between the number of high- and low-fidelity samples, model accuracy information needs to be obtained for many possible combinations. We gather such information by empirically performing a full enumeration of all possible combinations (n_l, n_h) for $2 < n_h < n_h^{\max}$ and $n_h + 1 < n_l < n_l^{\max}$. For each pair (n_l, n_h) we train multiple ($I = 50$) hierarchical multi-fidelity models to collect some statistics and evaluate the errors on an independent test set T . We refer to the tables of errors for the complete enumeration DoEs as *error grids*.

Algorithm 2 lists a pseudo-code representation of the procedure by which we obtain the error grids. The size of the test set T is set to $|T| = 500 \cdot N$, where N is the dimensionality of the search space (line 2). For each combination (n_h, n_l) , $I = 50$ independent DoEs

Algorithm 2 Full Enumeration Error Grid

Require: N -dimensional multi-fidelity problem (f_h, f_l)
Require: n_h^{\max}, n_l^{\max} \triangleright Maximum DoE size
Require: I \triangleright Number of iterations
1: $E \leftarrow \emptyset$ \triangleright Error Grid Storage
2: $T \leftarrow \text{LHS}(500 \cdot N)$ \triangleright Independent test set
3: **for** $n_h = 2 \dots n_h^{\max}$ **do**
4: **for** $n_l = (n_h + 1) \dots n_l^{\max}$ **do**
5: **for** $i = 1 \dots I$ **do**
6: $H, L \leftarrow \text{MF-LHS}(n_h, n_l)$ \triangleright Algorithm 1
7: $Y_h, Y_l \leftarrow f_h(H), f_l(L)$ \triangleright Evaluate
8: Train z_h using H, L, Y_h, Y_l
9: $E[n_h, n_l, i] \leftarrow \text{MSE}(z_h, T)$ \triangleright Equation (3.1)
10: **end for**
11: **end for**
12: **end for**
13: **return** E

are sampled and the errors for the multi-fidelity model based on each DoE are evaluated and stored (lines 5–10).

The resulting error between the surrogate model and the true high fidelity function can be visualized in heatmaps of the error grids as shown in Figure 4.1. We show the median error over the I independent realizations of the DoEs as 2D heatmaps and as function of H and L . These error grids serve as the basis for our analysis as we can:

- examine the dependence of the model error as function of the division ratio between the number of high- and low-fidelity evaluations;
- examine how this dependency varies between multi-fidelity problems; and
- identify the optimal division ratio for a given budget and problem.

However, the number of DoEs which need to be evaluated in this full enumeration procedure is $N_{\text{DoE}} = I n_h^{\max} (n_l^{\max} - n_h^{\max}/2)$, which for $I = 50$, $n_h^{\max} = 50$, $n_l^{\max} = 125$ is a total of $N_{\text{DoE}} = 250\,000$ DoEs to sample and models to train. The number of high-fidelity function evaluations is consequently in the millions, which might be feasible for trivially computable benchmark problems, but will be prohibitively infeasible for real-world problems with higher computational demand.

4.2 Cross-Validated Subsampling of DoE Sizes

In this section we describe how to approximate error grids using only one fixed initial multi-fidelity DoE. Given one DoE (H, L) with $n_h = |H|$ and $n_l = |L|$ samples, we can create a full error grid by reusing these evaluated samples and creating a set of smaller subsampled DoEs. Concretely, we subsample $H' \subset H, L' \subset L$ of size (n'_h, n'_l) such that the set of high fidelity samples H' is still a true subset of the set of low fidelity samples

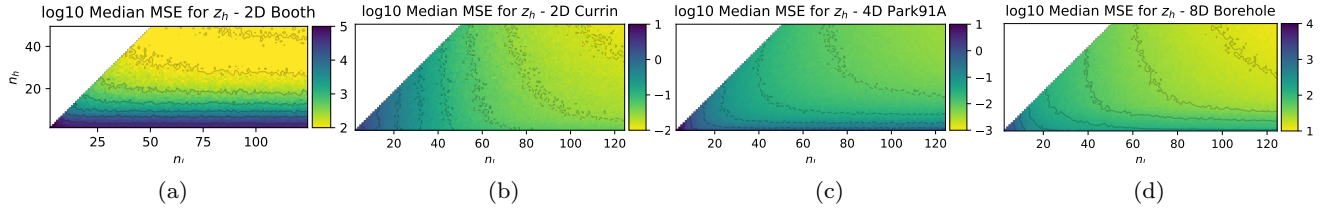


Fig. 4.1: **Error Grids** Heatmaps of the log 10 of the hierarchical model MSE for varying DoE sizes, shown as the median over $I = 50$ iterations, on four benchmark problems. Overall, it is clear that adding more samples improves model accuracy, either additional high-fidelity samples (vertical) or low-fidelity samples (horizontal)

L' , i.e., $H' \subset L'$. For this, we first draw H' uniformly at random without replacement from the available H . Then, we take those samples as a start for L' , and add randomly chosen low-fidelity points until the desired size is reached (see Algorithm 3).

Algorithm 3 Subsampling MF-DoE

```

Require: Initial multi-fidelity DoE ( $H, L$ )
Require: Desired DoE size  $n'_h, n'_l$ 
1:  $H' \leftarrow$  randomly choose  $n'_h$  samples from  $H$ 
2:  $L' \leftarrow$  randomly choose remaining  $n'_l - n'_h$  samples from  $(L \setminus H')$ 
3:  $L' \leftarrow L' \cup H'$ 
4: return  $H', L'$ 

```

Since the chosen high-fidelity DoE H' is a strict subset of the original DoE H , we can use some samples left out of the subsampled DoE H' to serve as test set $H^{\text{test}} = H \setminus H'$ and calculate the error of the surrogate models for each DoE similar to cross-validation. The complete subsampling approach is summarized in pseudocode shown in Algorithm 4.

Algorithm 4 Subsampling Error Grid Procedure

```

Require:  $N$ -dimensional multi-fidelity problem ( $f_h, f_l$ )
Require:  $I$  ▷ Number of iterations
1:  $E \leftarrow \emptyset$  ▷ Error Grid Storage
2:  $H, L \leftarrow \text{MF-LHS}(n_h^{\max}, n_l^{\max})$  ▷ Algorithm 1
3:  $Y_h, Y_l \leftarrow f_h(H), f_l(L)$  ▷ Evaluate once
4: for  $n_h = 2 \dots n_h^{\max} - 1$  do
5:   for  $n_l = (n_h + 1) \dots n_l^{\max}$  do
6:     for  $i = 1 \dots I$  do
7:        $H', L' \leftarrow \text{Subsample } H, L$  ▷ Algorithm 3
8:        $Y'_h, Y'_l \leftarrow \text{values from } Y_h, Y_l \text{ for } H', L'$ 
9:       Train  $z_h$  using  $H', L', Y'_h, Y'_l$ 
10:       $E[n_h, n_l, i] \leftarrow \text{MSE}(z_h, H^{\text{tst}})$  ▷  $H^{\text{tst}} : H \setminus H'$ 
11:    end for
12:  end for
13: end for
14: return  $E$ 

```

4.3 Angle of Gradient Quantification

The error grids provide intuitive information about the trade-off between the numbers of high- and low-fidelity samples. The contour lines give a very clear visual guidance in which direction of the (n_h, n_l) -plane the accuracy of the surrogate models increases. To evaluate this behavior quantitatively, we use the gradient of the error with respect to the number of samples. If this gradient direction is predominantly along the n_h direction, i.e., it has an angle close to 90° as measured from the horizontal n_l axis (see example in Figure 4.1), this indicates that improvements in model quality mostly depend on additional high-fidelity information. However, if the error gradient angle is more horizontal, the benefit of adding low-fidelity information is larger. It is important to note that even when the angle is mostly vertical, e.g., 80° , adding low-fidelity information can still be beneficial as long as it is computationally much cheaper.

In the following we utilize the direction of the error gradient to estimate the best split between high and low fidelity samples in order to reduce the modeling error. Even though the error gradient varies strongly depending on the actual number of high- and low-fidelity samples, we can extract the global behavior by employing a linear fit of a hyperplane through the \log_{10} of the MSE data according to

$$\log_{10}(MSE) = \alpha + \beta_h n_h + \beta_l n_l \quad (4.1)$$

This is of course a very crude approximation to the actual, nonlinear behavior of the MSE, and in general a more complicated nonlinear function could be used. However, the general framework presented in this work is independent of the actual fit formula or the way how the gradient direction is extracted. We utilize this linear fit due to its simplicity and, as we will see, it can already provide strong benefits.

From the linear fit, the global direction of the gradient direction of reducing error can be summarized intuitively by an angle

$$\theta = \arctan \left(\frac{\beta_h}{\beta_l} \right). \quad (4.2)$$

For the error grids in Figure 4.1, for example, this results in angles of $\theta_{\text{Booth}(2D)} \approx 88^\circ$, $\theta_{\text{Currin}(2D)} \approx 34^\circ$, $\theta_{\text{Park91A}(4D)} \approx 72^\circ$ and $\theta_{\text{Borehole}(8D)} \approx 63^\circ$, respectively.

From the linear fit of equation (4.1) we can also calculate the standard errors for the linear fit parameters β_i associated with input feature n_i , i.e., the number of high- or low-fidelity samples n_h or n_l , as

$$se_{\beta_i} = \frac{\sqrt{\frac{\text{SSE}}{N_{\text{DoE}} - df}}}{\sqrt{\sum(n_i - \bar{n}_i)^2}} = \frac{\sqrt{\sum(f_h(x) - z_h(x))^2}}{\sqrt{\sum(n_i - \bar{n}_i)^2}}, \quad (4.3)$$

where n_i can either be the number of high- or low-fidelity samples, \bar{n}_i is the respective mean, df is the number of degrees of freedom, i.e., the number of samples N_{DoE} minus three for the number of parameters from the linear regression equation $(\alpha, \beta_h, \beta_l)$, and SSE is the sum of squared errors for our linear fit.

Using these standard errors we can determine a 95% Confidence Interval (CI) for the slope $\frac{\beta_h}{\beta_l}$, from which we can estimate the range of the angle:

$$\text{CI } \frac{\beta_h}{\beta_l} = \frac{\beta_h}{\beta_l} \pm 1.96 \sqrt{\left(\frac{se_{\beta_h}}{\beta_h}\right)^2 + \left(\frac{se_{\beta_l}}{\beta_l}\right)^2} \quad (4.4)$$

$$\begin{aligned} \text{CI } \theta \approx & \left[\tan^{-1} \left(\frac{\beta_h}{\beta_l} - 1.96 \sqrt{\left(\frac{se_{\beta_h}}{\beta_h}\right)^2 + \left(\frac{se_{\beta_l}}{\beta_l}\right)^2} \right), \right. \\ & \left. \tan^{-1} \left(\frac{\beta_h}{\beta_l} + 1.96 \sqrt{\left(\frac{se_{\beta_h}}{\beta_h}\right)^2 + \left(\frac{se_{\beta_l}}{\beta_l}\right)^2} \right) \right] \quad (4.5) \end{aligned}$$

Using this CI, we can be more certain of the global error gradient angle of the error grid. In any local section of the error grid, the angle can still be significantly different, but the proposed method provides a robust estimate of the average gradient and serves the purpose of discriminating the global behavior of different benchmark functions.

5 Experiments

5.1 Replication of results and implementation details

All source code of this work is available on GitHub [19], and archived on Zenodo [20, 23] together with (processed) data files. The analyses are written in Python 3.6+ and reproducibility is guaranteed by using a single fixed random seed for globally used random values such as the test set T and the initial DoE used for subsampling. For all instance-specific random values, random seeds are fixed to zero-padded concatenations of n_h , n_l and the repetition index. All experiments use $I = 50$ iterations unless otherwise noted.

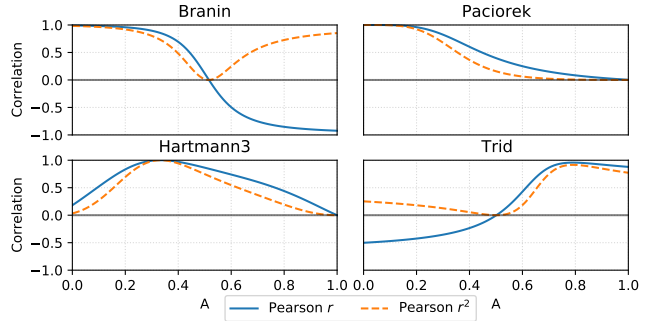


Fig. 5.1: Correlation between high- and low-fidelity for adjustable 2D Branin, 2D Paciorek, 3D Hartmann3 and 10D Trid functions as function of parameter A  

For the Gaussian Process-based surrogate models, we use the scikit-learn implementation [17], and we use benchmark function implementations from version 2021.2.0 of the `mf2` package [21]. Other core packages upon which this research is built are Numpy [27], Matplotlib [11], and xarray [9]. All other dependencies are listed in the `requirements.txt` of the code repository.

5.2 Benchmark functions

The used benchmark functions from the `mf2` package range from one dimensional (1D), such as the Forrester function, to 10D such as the Trid function, with a majority of 2D functions such as Bohachevsky, Currin and Six-Hump Camelback. This collection contains several different problem landscapes and all are previously used in the literature. With the exception of the 2D Branin function, the Pearson correlation between their high- and low-fidelity functions are all above 0.7.

In particular, we focus on the adjustable benchmark functions previously proposed by Toal in Section 3 of [26]: the 2D *adjustable* Branin¹, 2D Paciorek, 3D Hartmann3, and the 10D Trid function. The low-fidelity functions of these benchmarks include a tuning parameter A , which controls the correlation between high- and low-fidelity for these functions. Figure 5.1 shows the relationship between A and the Pearson correlation for these functions. For all functions, correlation can be tuned to any value between maximally positive ($r \approx 1$) and absent ($r \approx 0$). Additionally, for the Branin and Trid functions, this range extends to negative correlations ($r \approx -1$). The explicit functional forms can be found in the paper by Toal [26] or in the implementation of the `mf2` package [21].

¹ Since Toal's adjustable Branin function differs from the non-adjustable version by Dong *et al.* [2], we explicitly differentiate between them by referring to Toal's version as the *adjustable* Branin function

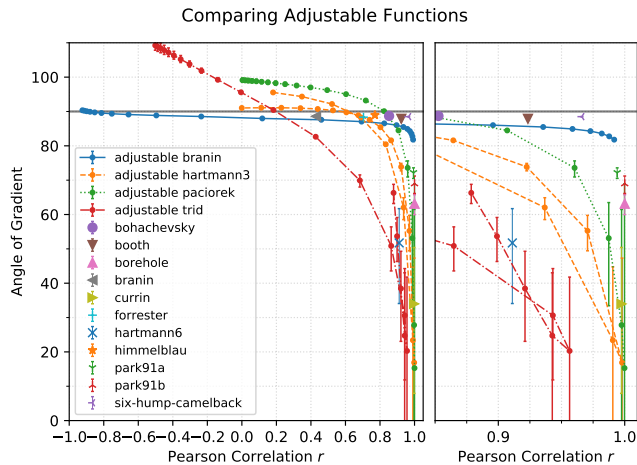


Fig. 5.2: **Angle as function of correlation** illustrated for all functions in the `mf2` [21] package. The left side shows the complete range $-1 \leq r \leq 1$, while the right side highlights the highly correlated region $0.85 \leq r \leq 1$. Single markers are used for non-adjustable functions such as Booth. Lines with markers show various parameter values for the adjustable functions where the line connects points with adjacent values of A . Error bars show the CI as defined in Equation (4.5)  

5.3 Error Gradient Angle Analysis

The full enumeration procedure described in Section 4.1 was run for each of the four adjustable functions, with parameter values $A \in [0, 0.05, \dots, 0.95, 1.0]^2$. For all the adjustable as well as the non-adjustable functions the gradient direction and error gradient angle was estimated using the linear fit procedure described in Section 4.3. The resulting angles, along with the confidence intervals, are shown in Figure 5.2 as function of the Pearson correlation r .

First, it should be noted that the calculated angles cover a very wide range from basically zero up to almost 120 degrees, with the bulk of the values between 30 and 90 degrees. For many functions and in a large range of correlations an angle of around 90° is computed, which indicates that the accuracy only increases when adding high fidelity samples. Interestingly, angles $\geq 90^\circ$ are also present. These high angles indicate that the added low-fidelity information actually hurts the accuracy of this hierarchical model, making it perform *worse* than a model trained with fewer low-fidelity samples. This adverse effect of increasing the error by adding low-fidelity samples occurs for correlations up to $r \lesssim 0.8$ and the tendency gets stronger for less correlated or

² Except for the Paciorek function, where the high- and low-fidelity versions are identical for $A = 0$.

even anti-correlated benchmark functions. It should be noted that this is not an artifact of the linear fit or the way the error gradient angles are calculated, but truly reflects the behavior of the model error for those functions, as can be seen in Figure 5.3 for the adjustable Trid function.

It is clear from Figure 5.2 that there is a strong relationship between correlation coefficients and the error gradient angle. For each function, there is a strong tendency to get lower angles with increasing correlation coefficient. However, the absolute numbers and the functional relationship differ vastly. Even for high correlation coefficients, e.g., $r \geq 0.9$, a large range of resulting error gradient angles can be observed. This means that a high correlation does not necessarily imply a low error gradient angle in the corresponding error grid.

Furthermore, the Hartmann3 and Trid functions show some other interesting behavior. Note from Figure 5.1 that within A 's parameter range (i.e., $[0, 1]$), the correlation for the Hartmann3 and Trid functions rises to a maximum and drops off again after that for both these functions. A direct consequence of this is that there are correlation ranges where there are two lines for the Hartmann3 and Trid functions visible in Figure 5.2. Following the curves of those functions from low to high and back to lower values of r in Figure 5.2 shows that the error gradient angles also first decrease and then increase again. Such behavior is confirmed by inspecting the error grids directly as shown in Figure 5.3.

These examples show that despite the fact that only a linear fit is used to extract gradient direction, the overall functional dependency of the model error is captured rather well. Other, more complicated measures for the relation between the multi-fidelity samples and for estimating the gradient direction are more accurate and could capture local variations of the directions, but for the purpose of this work these are not necessary. The proposed linear measures are accurate enough to capture the global tendencies and already allow for insightful improvements and the possibility to formulate useful heuristics for practical application (see below).

5.4 Subsampling Analysis

To validate our proposed method of reducing the number of necessary function evaluations for the error grid analysis described in Section 4.2, we explore the influence of the sizes of training and test sets. Results of the following three setups are compared:

1. Independent full enumeration of training and test sets as described in Section 4.1;
2. Subsampled training set and independent test set;

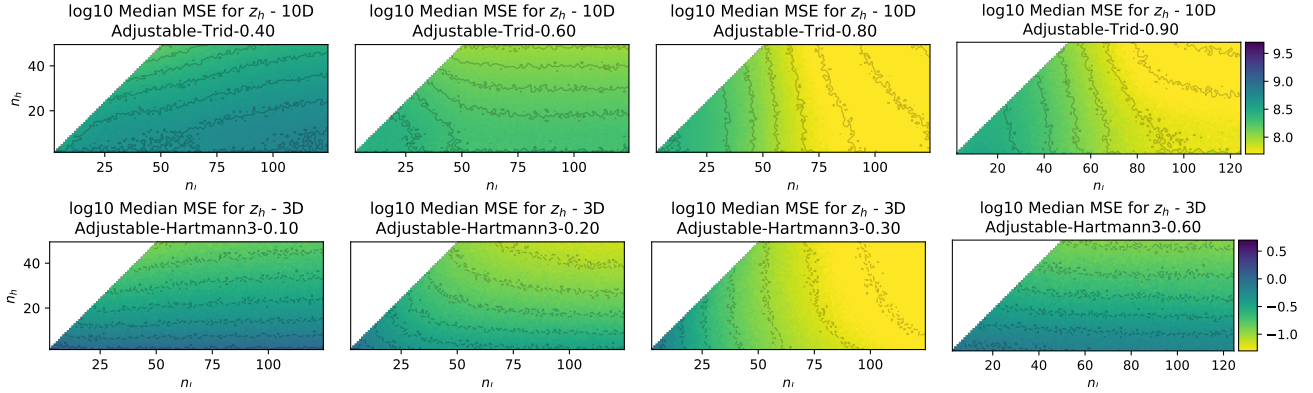


Fig. 5.3: Error grids for adjustable Trid function for $A = 0.4, 0.6, 0.8, 0.9$, with $r = -0.23, 0.43, 0.96, 0.92$, respectively (upper row, from left to right) and the adjustable Hartmann3 function for $A = 0.1, 0.2, 0.3, 0.6$, with $r = 0.54, 0.84, 0.99, 0.74$, respectively (lower row, from left to right)  

Function	Parameter values used for A_1, \dots, A_4
Branin	0.00, 0.05, 0.25
Paciorek	0.05, 0.10, 0.15, 0.20, 0.25
Hartmann3	0.20, 0.25, 0.30, 0.35, 0.40
Trid	0.65, 0.70, 0.75, 0.80, 0.85, 0.90, 0.95, 1.00

Table 5.1: Listing of all parameters that are used to compare correlation between error gradient angles from full enumeration and subsampling

3. Subsampled training set and left-over test set, i.e., full subsampling as described in Section 4.2

If accurate enough, the third setup is the preferred approach for practical applications, as it uses any computational budget most efficiently by using each available evaluation for either test or training sets, and no further evaluations besides that.

Comparing between 1. and 2. shows the dependence of the procedure's results on the initial DoEs used as training set: does the spread of the subsamples cover the search space well enough to simulate independent DoEs of the subsample size? The comparison between 2. and 3. illustrates how accuracy tests with (much) less information influence the results.

Figure 5.4 shows example comparisons for the adjustable Branin, Hartmann3 and Trid functions. The ground-truth error grid (left) shows a mostly 90° gradient for $n_l \gg n_h$ with a trend toward 45° near the $n_h = n_l$ diagonal. The subsampling error grids (middle and right panels) are visibly noisier than the ground-truth, but show similar shape characteristics. Despite the subtle differences in curvature, the resulting error gradient angles are very similar between 80° - 82° .

For a more detailed analysis, we select 21 (function, parameter) combinations as described in Table 5.1 that

cover a wide range of error gradient angles. For all cases, both subsampling procedures are repeated five times using independent initial DoEs in each case, and the error gradient angles are calculated. Figure 5.5 shows the correlation between the angles from the full enumeration and the subsampling procedures, as evaluated using both the independent large test set (left) and with the full subsampling approach with left-over test set (right).

First considering Figure 5.5a, we see that the angles from subsampling correspond very well to the ground-truth angles, with a spread of $\pm 5^\circ$ to $\pm 15^\circ$ roughly symmetrically around diagonal. The magnitude of the spread is visibly larger as the angles are smaller.

Figure 5.5b compares the ground-truth error gradient angles with those calculated using the test set based on cross-validation. Again, the variance in the estimated angle becomes smaller for larger angles. It is interesting to note that the spreads of the angles are also roughly between $\pm 5^\circ$ to $\pm 15^\circ$, but there seems to be a systematic shift of the angles estimated by full subsampling with a cross-validated test set to *higher* values. The exact shift is dependent on the underlying function, e.g. the Paciorek function having a much larger shift than the Hartmann3 function. So while not an exact prediction of the ground-truth error gradient angle, it can be interpreted as a worst-case estimate: the ground-truth error gradient angle is unlikely to be higher than what results from this procedure.

5.5 Extrapolation

Given that the error grids from subsampling and their subsequent error gradient angles have been shown to match those from full enumeration quite well, we propose using this information to answer the question posed in

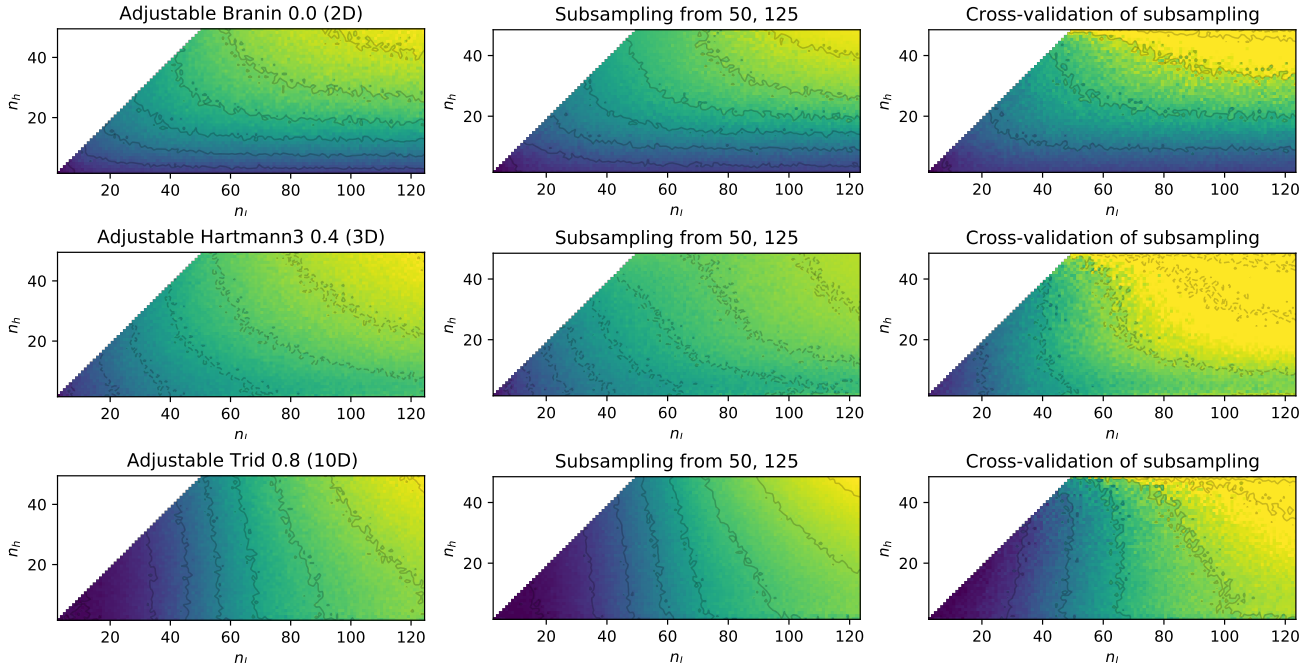


Fig. 5.4: **Comparison of error grids** for the Adjustable Branin ($A = 0.0$, $r = 0.99$), Hartmann3 ($A = 0.4$, $r = 0.97$), and Trid ($A = 0.8$, $r = 0.96$) using different methods. **Left:** error results using independent training and test set (Section 4.1). The estimated error gradient angles are $\theta = 81.8^\circ$, 55.4° , 20.4° . **Middle:** error results using subsampled training set, with independent test set. The estimated error gradient angles are $\theta = 80.3^\circ$, 54.0° , 25.5° . **Right:** error results using subsampled training set and left-over test set (Section 4.2). The estimated error gradient angles are $\theta = 81.7^\circ$, 58.0° , 32.2° .  

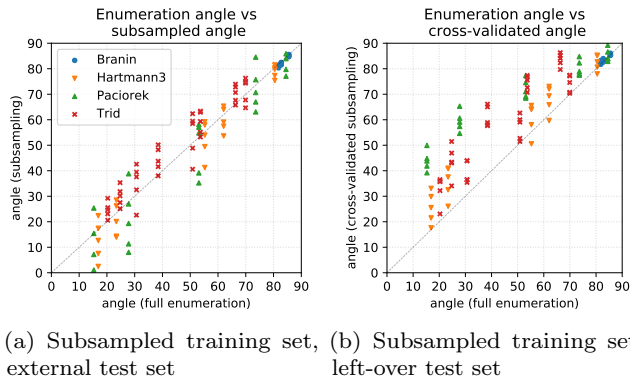


Fig. 5.5: **Error gradient angle correlation** The horizontal axis shows the angles as determined using the full enumeration procedure, while the vertical axis shows the angles calculated by the procedure as mentioned by the caption below each figure  

Section 3: how should additional computation budget be divided between the two available fidelity levels?

From the linear regression fit of a given error grid and the resulting gradient direction as described in Section 4.3, the relation between number of low and

high fidelity samples which gives the best reduction in model error is given by

$$\frac{n_h}{n_l} = \frac{\beta_h}{\beta_l} \quad (5.1)$$

When increasing the number of samples from a given initial DoE with number of samples $(n_{h,0}, n_{l,0})$ to a final DoE with samples (n_h, n_l) , the additional number of samples should be along the direction of the gradient line through the point $(n_{h,0}, n_{l,0})$ and therefore respect the relation

$$\Delta n_h = \frac{\beta_h}{\beta_l} \Delta n_l \quad (5.2)$$

where $\Delta n_h = n_h - n_{h,0}$ and $\Delta n_l = n_l - n_{l,0}$ are the additional samples to be simulated. A fixed additional budget b can be split between high and low fidelity samples according to the cost ratio ϕ ,

$$\Delta n_h + \phi \Delta n_l = b. \quad (5.3)$$

From Equations (5.2) and (5.3) we can determine the best number of additional low and high fidelity samples for a given additional computational budget b as

$$\Delta n_l = \frac{b \beta_l}{\beta_h + \phi \beta_l} \quad (5.4)$$

$$\Delta n_h = \frac{b \beta_h}{\beta_h + \phi \beta_l}. \quad (5.5)$$

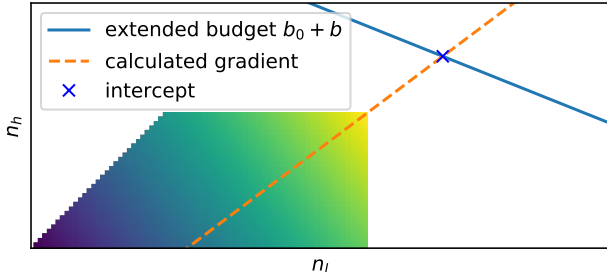


Fig. 5.6: Schematic representation of the proposed method to determine the best split for a given additional budget b by extrapolating along the gradient of the error grid until it intersects. Cost ratio for this example is $\phi = 0.4$

Figure 5.6 shows the schematic representation of the proposed extrapolation method for splitting an additional budget b . The orange line indicates the extension of the error grid along the direction of the gradient of the error grid. The blue line represents the line where the additional budget is spent according to the cost ratio. The intersection of both lines marks the proposed new samples split for the next DoE. Notice that the initial sample sizes $(n_{h,0}, n_{l,0})$ do not need to respect the cost ratio relation of Equation (5.3), as the initial DoE might be obtained by any method.

We evaluate the accuracy of the proposed extrapolation method by considering an initial DoE for all different benchmark functions with $(n_{h,0}, n_{l,0}) = (30, 75)$ samples, an assumed cost ratio of $\phi = 0.4$ and an additional computational budget of $b = 20$. We calculate the error grid and the corresponding gradient direction by the cross-validated subsampling procedure of Section 4.2. We then evaluate the error of the hierarchical model by the full enumeration procedure for all points along the line of constant additional budget (corresponding to the orange line in Figure 5.6) and compare it to the sample split proposed by Equation (5.4). Figure 5.7 shows the results of this procedure where the position along the constant additional budget line and the proposed sample split is characterized by the angle measured from the position $(n_{h,0}, n_{l,0}) = (30, 75)$ of the initial DoE.

Generally, it can be observed that the MSE values are quite noisy, even though the median MSE values of 50 different runs are plotted. This is due to the fact that the total number of samples is rather low for the investigated functions, leading to generally large error and also large variations in error. But since we are ultimately interested in real-world problems, where low number of (high fidelity) samples is the norm, we choose such a setup as such noise is expected in these scenarios. From the plots it can be observed that the first three

examples show that the predicted best angle, i.e., error gradient angle from the subsampled error grid, matches roughly with the minimum MSE along the constant budget line, regardless of whether this angle is high (90°) or low (0°). However, the last plot shows a case where the predicted angle does not lead to a region of low error but rather high error. This is likely an artifact of the linear fit to the error grid. If the function has different characteristics for the region of low samples compared to the number of high samples, the linear fit matches the low-sample region and cannot accurately describe the region larger number of samples where the extrapolation is done. So the global estimate of the gradient of the error grid does not align with the local direction of decreasing error around the position of the initial DoE. This is the case for the Park91A function shown in Figure 4.1c and Figure 5.7. The error grid of the initial DoE with $(n_{h,0}, n_{l,0}) = (30, 75)$ is best fit by a linear function with a rather large 75° error gradient angle and consequently the extrapolation suggest to sample $(\Delta n_{h,0}, \Delta n_{l,0}) = (17, 7)$ additional points corresponding to that angle. However, only looking at the region above and to the right of the initial DoE with $(n_{h,0}, n_{l,0}) = (30, 75)$ in the error grid of Figure 4.1c reveals that the direction of decreasing error is more along the n_l axis., i.e. for angles close to zero.

This shortcoming of the extrapolation used to determine the split of an additional budget could be mitigated by either not using a linear fit to determine the global gradient direction, but a more complex function. However, this function then would need to be able to fit the error grid better and also extrapolate well to the unseen region above the initial DoE. Alternatively, and probably more appropriate would be to retain the linear fit due to its simplicity and robustness but limit the region of the error grid to which the fit is done to a smaller neighborhood of the initial DoE size. Then the local trend would most likely be captured better and the extrapolation would better match the local direction of the gradient.

6 Conclusions

In this work we have empirically examined the trade-off that exists in dividing computational budget between high- and low-fidelity samples in the context of multi-fidelity modeling and optimization problems.

We presented the so-called error grids which are given by the modeling error of a hierarchical surrogate model for a DoE with a given number of high and low fidelity samples (n_h, n_l) . For a complete error grid the modeling error is evaluated for a multitude of DoEs with sample points (n'_h, n'_l) up to the size of the initial DoE,

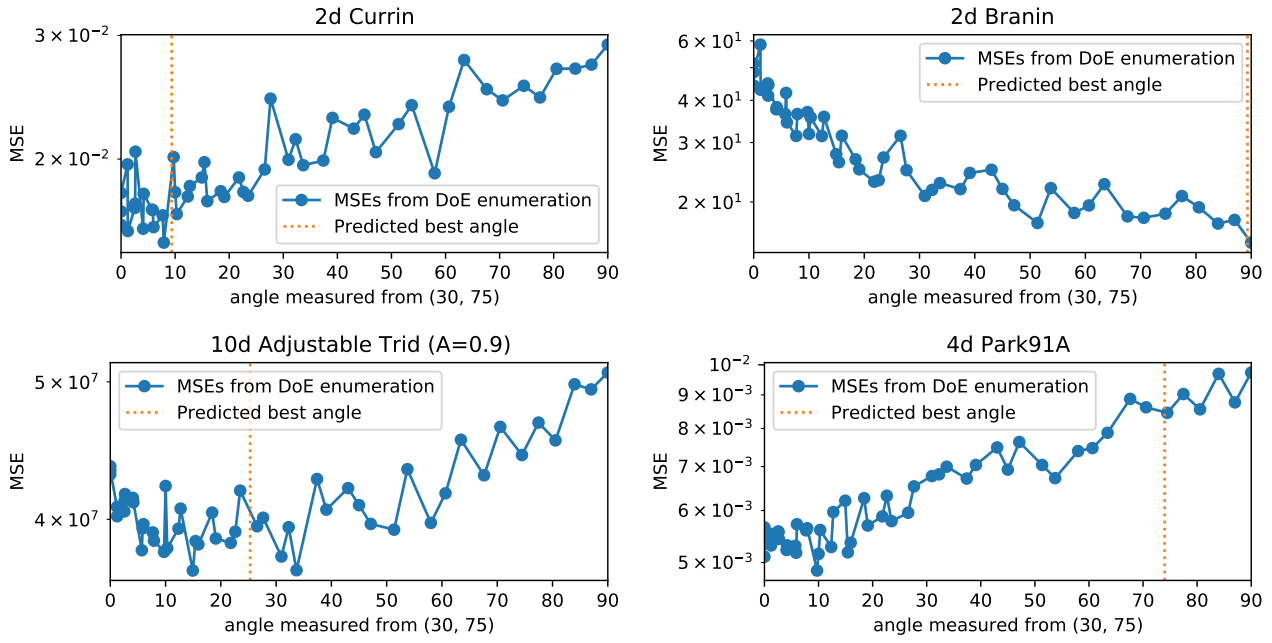


Fig. 5.7: Median \log_{10} MSE of DoE sizes along line $b = n_h + \phi n_l = 80$ (given $\phi = 0.4$) in the fully enumerated error grid (i.e. without subsampling), shown on the x-axis as the angle measured from the initial sample point $(n_{h,0}, n_{l,0}) = (30, 75)$ for four benchmark functions. The dashed vertical line shows the angle for the proposed new sample split as calculated by Equation (5.4)  

i.e. DoE (n'_h, n'_l) with $n'_h \in [2, n_h]$ and $n'_l \in [n'_h, n'_l]$. By this the structure of the model error is revealed and the behavior of the modeling error as function of the split between high and low fidelity samples can be analyzed.

We captured the global trend in the modeling error by fitting a linear hyperplane through the \log_{10} of the Mean Squared Errors. The linear fit easily lends itself to extracting the global direction of error gradient which is used to identify the global direction of reducing error in the n_h - n_l plane. We analyzed the error grids for a multitude of benchmark functions, where some functions have a parameter which allows to tune the relation between low and high fidelity functions.

The first version of the error grid we presented utilizes an independently sampled DoE for each hierarchical model with a given sample split. This requires a very large number of independent function evaluations and we therefore presented a simple subsampling method which utilized only the available evaluations of one initial DoE in the spirit of cross-validation. We showed for multiple benchmark functions that the direction of the gradient of the error grid can be estimated from the subsampling error grid reasonably well.

Based on the extracted global direction of the gradient of the modeling error, we proposed a simple scheme which allows an informed decision about how to divide additionally available evaluation budget between the

different fidelities. We showed that the scheme works well on most benchmark functions. Those cases where the predicted split of the additional budget did not extrapolate to a region with smaller model error are characterized by a change of the dominant behavior of the function with the number of high- and low-fidelity samples. This shortcoming of the proposed method could be mitigated by performing the linear fit only to a local region around the current DoE's sample sizes.

In future work, experiments on additional benchmark functions and also real-world problems will have to be performed in order to qualify the benefits of the error grids for those applications. As we have only considered a hierarchical surrogate model based on the simple additive co-kriging design, other multi-fidelity models should be investigated.

Also, the presented extrapolation scheme should be employed in multi-fidelity optimization settings, as they continuously face the challenge of deciding in which fidelity to evaluate the next sample. In each optimization iteration, additional computational budget needs to be distributed to the evaluation of newly proposed candidate solutions, and determining the best split between high and low fidelity samples to most efficiently reduce the modeling error should be beneficial to the optimization progress.

Conflict of Interest

On behalf of all authors, the corresponding author states that there is no conflict of interest.

Acknowledgements

This work is part of the research program DAMIOSO, project number 628.006.002, which is partly financed by the Netherlands Organisation for Scientific Research (NWO).

References

1. Belakaria, S., Deshwal, A., Doppa, J.R.: Multi-Fidelity Multi-Objective Bayesian Optimization: An Output Space Entropy Search Approach. *Proceedings of the AAAI Conference on Artificial Intelligence* **34**(06), 10035–10043 (2020). [doi:10.1609/aaai.v34i06.6560](https://doi.org/10.1609/aaai.v34i06.6560)
2. Dong, H., Song, B., Wang, P., Huang, S.: Multi-fidelity Information Fusion Based on Prediction of Kriging. *Structural and Multidisciplinary Optimization* **51**(6), 1267–1280 (2015). [doi:10.1007/s00158-014-1213-9](https://doi.org/10.1007/s00158-014-1213-9)
3. Douglas C. Montgomery: Design and Analysis of Experiments, 10 edn. Wiley (2019). URL <https://www.wiley.com/en-us/Design+and+Analysis+of+Experiments%2C+10th+Edition-p-9781119492443>
4. Durantin, C., Rouxel, J., Désidéri, J.A., Glière, A.: Multi-fidelity surrogate modeling based on radial basis functions. *Structural and Multidisciplinary Optimization* **56**(5), 1061–1075 (2017). [doi:10.1007/s00158-017-1703-7](https://doi.org/10.1007/s00158-017-1703-7)
5. Fernández-Godino, M.G., Dubreuil, S., Bartoli, N., Balachandar, S., Haftka, R.T.: Linear Regression Based Multi-fidelity Surrogate for Disturbance Amplification in Multi-phase Explosion. *Structural and Multidisciplinary Optimization* pp. 2205–2220 (2019). [doi:10.1007/s00158-019-02387-4](https://doi.org/10.1007/s00158-019-02387-4)
6. Fernández-Godino, M.G., Park, C., Kim, N.H., Haftka, R.T.: Review of multi-fidelity models. arXiv:1609.07196 [stat] p. 46 (2016). URL [http://arxiv.org/abs/1609.07196](https://arxiv.org/abs/1609.07196)
7. Forrester, A.I.J., Sobester, A., Keane, A.J.: Multi-fidelity optimization via surrogate modelling. *Proceedings of the Royal Society of London A: Mathematical, Physical and Engineering Sciences* **463**(2088), 3251–3269 (2007). [doi:10.1098/rspa.2007.1900](https://doi.org/10.1098/rspa.2007.1900)
8. Guo, Q., Hang, J., Wang, S., Hui, W., Xie, Z.: Design optimization of variable stiffness composites by using multi-fidelity surrogate models. *Structural and Multidisciplinary Optimization* (2020). [doi:10.1007/s00158-020-02684-3](https://doi.org/10.1007/s00158-020-02684-3)
9. Hoyer, S., Hamman, J.: xarray: N-D labeled Arrays and Datasets in Python. *Journal of Open Research Software* **5**(1), 10 (2017). [doi:10.5334/jors.148](https://doi.org/10.5334/jors.148). Number: 1 Publisher: Ubiquity Press
10. Huang, D., Allen, T.T., Notz, W.I., Miller, R.A.: Sequential kriging optimization using multiple-fidelity evaluations. *Structural and Multidisciplinary Optimization* **32**(5), 369–382 (2006). [doi:10.1007/s00158-005-0587-0](https://doi.org/10.1007/s00158-005-0587-0)
11. Hunter, J.D.: Matplotlib: A 2D Graphics Environment. *Computing in Science Engineering* **9**(3), 90–95 (2007). [doi:10.1109/MCSE.2007.55](https://doi.org/10.1109/MCSE.2007.55). Conference Name: Computing in Science Engineering
12. Kennedy, M.C., O'Hagan, A.: Predicting the output from a complex computer code when fast approximations are available. *Biometrika* **87**(1), 1–13 (2000). [doi:10.1093/biomet/87.1.1](https://doi.org/10.1093/biomet/87.1.1)
13. Le Gratiet, L.: Multi-fidelity Gaussian process regression for computer experiments. Ph.D. thesis, Sorbonne Université (2013). URL <https://tel.archives-ouvertes.fr/tel-00866770/>
14. Li, N., Lee, E.W.M., Cheung, S.C.P., Tu, J.: Multi-fidelity surrogate algorithm for fire origin determination in compartment fires. *Engineering with Computers* (2019). [doi:10.1007/s00366-019-00738-9](https://doi.org/10.1007/s00366-019-00738-9)
15. Liu, Y., Chen, S., Wang, F., Xiong, F.: Sequential optimization using multi-level cokriging and extended expected improvement criterion. *Structural and Multidisciplinary Optimization* **58**(3), 1155–1173 (2018). [doi:10.1007/s00158-018-1959-6](https://doi.org/10.1007/s00158-018-1959-6)
16. Moss, H.B., Leslie, D.S., Rayson, P.: MUMBO: Multi-task Max-value Bayesian Optimization. arXiv:2006.12093 [cs, stat] (2020). URL [http://arxiv.org/abs/2006.12093](https://arxiv.org/abs/2006.12093)
17. Pedregosa, F., Varoquaux, G., Gramfort, A., Michel, V., Thirion, B., Grisel, O., Blondel, M., Prettenhofer, P., Weiss, R., Dubourg, V., Vanderplas, J., Passos, A., Cournapeau, D., Brucher, M., Perrot, M., Duchesnay, ..: Scikit-learn: Machine Learning in Python. *Journal of Machine Learning Research* **12**, 2825–2830 (2011). URL <http://jmlr.csail.mit.edu/papers/v12/pedregosa11a.html>
18. Pellegrini, R., Iemma, U., Leotardi, C., Campana, E.F., Diez, M.: Multi-fidelity adaptive global metamodel of expensive computer simulations. In: 2016 IEEE Congress on Evolutionary Computation (CEC). Vancouver (2016). [doi:10.1109/CEC.2016.7744355](https://doi.org/10.1109/CEC.2016.7744355)
19. van Rijn, S.: Multi-Level-Co-Surrogates (2020). URL <https://github.com/sjvrijn/multi-level-co-surrogates>
20. van Rijn, S.: sjvrijn/multi-level-co-surrogates: v1 (2021). [doi:10.5281/zenodo.4552822](https://doi.org/10.5281/zenodo.4552822)
21. van Rijn, S., Schmitt, S.: MF2: A Collection of Multi-Fidelity Benchmark Functions in Python. *Journal of Open Source Software* (2020). [doi:10.21105/joss.02049](https://doi.org/10.21105/joss.02049)
22. van Rijn, S., Schmitt, S., van Leeuwen, M., Bäck, T.: Full size figures in this paper (2021). [doi:10.6084/m9.figshare.c.5311481.v2](https://doi.org/10.6084/m9.figshare.c.5311481.v2)
23. van Rijn, S., Schmitt, S., van Leeuwen, M., Bäck, T.: Generated data files and figures (2021). [doi:10.5281/zenodo.4551287](https://doi.org/10.5281/zenodo.4551287)
24. Ryou, G., Tal, E., Karaman, S.: Multi-Fidelity Black-Box Optimization for Time-Optimal Quadrotor Maneuvers. arXiv:2006.02513 [cs] (2020). URL [http://arxiv.org/abs/2006.02513](https://arxiv.org/abs/2006.02513)
25. Shi, R., Liu, L., Long, T., Wu, Y., Gary Wang, G.: Multi-Fidelity Modeling and Adaptive Co-Kriging-Based Optimization for All-Electric Geostationary Orbit Satellite Systems. *Journal of Mechanical Design* **142**(2) (2020). [doi:10.1115/1.4044321](https://doi.org/10.1115/1.4044321)
26. Toal, D.J.J.: Some considerations regarding the use of multi-fidelity Kriging in the construction of surrogate models. *Structural and Multidisciplinary Optimization* **51**(6), 1223–1245 (2015). [doi:10.1007/s00158-014-1209-5](https://doi.org/10.1007/s00158-014-1209-5)
27. van der Walt, S., Colbert, S.C., Varoquaux, G.: The NumPy Array: A Structure for Efficient Numerical Computation. *Computing in Science Engineering Conference* **13**(2), 22–30 (2011). [doi:10.1109/MCSE.2011.37](https://doi.org/10.1109/MCSE.2011.37)
28. Zhou, X., Hsieh, S.J., Wang, J.C.: Accelerating extrusion-based additive manufacturing optimization processes with surrogate-based multi-fidelity models. *The International Journal of Advanced Manufacturing Technology* **103**(9), 4071–4083 (2019). [doi:10.1007/s00170-019-03813-z](https://doi.org/10.1007/s00170-019-03813-z)